

# Field-induced Kitaev multipolar liquid in spin-orbit coupled $d^2$ honeycomb Mott insulators

Ahmed Rayyan,<sup>1</sup> Derek Churchill,<sup>1</sup> and Hae-Young Kee<sup>1,2,\*</sup>

<sup>1</sup>*Department of Physics, University of Toronto, Toronto ON M5S 1A7, Canada*

<sup>2</sup>*CIFAR Program in Quantum Materials, Canadian Institute for Advanced Research, Toronto ON M5G 1M1, Canada*  
(Dated: March 8, 2023)

The Kitaev model, characterized by bond-dependent Ising spin interactions among spin-orbit entangled dipole moments in Mott insulators, offered a new approach to quantum spin liquids. Motivated by another type of bond-dependent interaction among quadrupole moments in  $5d^2$  Mott insulators, we provide a microscopic route to uncover the Kitaev multipolar liquid, featuring fractionalized excitations out of non-Kramers doublets carrying multipole moments. The key ingredient is the magnetic field that allows for bond-anisotropic quadrupole-octupole interactions via mixing with the excited triplet states. The conditions to realize signatures of this phase in real materials are also discussed.

*Introduction*—Recently, there have been many studies on candidate materials of Kitaev spin liquids (KSLs) as they offer a platform for topological quantum computation [1, 2]. The Kitaev honeycomb model consists of bond-dependent Ising interactions leading to the KSL with Majorana fermion and  $\mathbb{Z}_2$  vortex excitations. It was shown that bond-dependent (or “compass”) interactions appear naturally in Mott insulators with strong spin-orbit coupling since the spin sector of the localized wavefunctions becomes sensitive to the orbital spatial orientation due to spin-orbit entanglement [3–12]. Since then there has been an intensive search for candidate Kitaev materials described by an effective model of spin-orbit entangled  $J_{\text{eff}} = 1/2$  Kramers doublets [3, 4, 9, 13–31].

Bond-dependent interactions are not limited to Kramers doublets; in the  $5d^2$  double perovskites, the  $J = 2$  states are further split into a non-Kramers doublet and an excited triplet via  $t_{2g}$ - $e_g$  mixing [32–34]. The non-Kramers doublet hosts quadrupole and octupole moments while lacking a dipole moment, and the microscopic theory of the multipolar interactions exhibit octupole-octupole and bond-dependent quadrupole-quadrupole interactions [35–37]. Remarkably, such interactions on the honeycomb lattice take the form of the extended Kitaev model, which includes the bond-dependent off-diagonal exchanges  $\Gamma$  and  $\Gamma'$  along with the conventional Heisenberg interaction. Given their similarity, one may question if there is a way to realize the exactly-solvable Kitaev model in multipolar honeycomb systems.

In this Letter, we present a microscopic theory to uncover the Kitaev model among multipolar moments where non-Kramers doublets are fractionalized into Majorana fermions and  $\mathbb{Z}_2$  vortices; we call this phase the *Kitaev multipolar liquid* in analogy with the KSL. The key ingredient to realize the KML is the application of a magnetic field which leads to bond-dependent quadrupole-octupole interactions ordinarily forbidden by time-reversal symmetry. Below we first derive the low-energy effective multipolar model including the time-reversal symmetry breaking terms and present its classi-

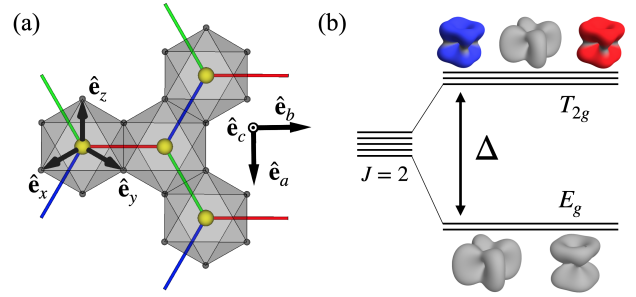


Figure 1. (a) The honeycomb lattice with transition metal ions (shown in yellow) enclosed in an octahedral anion cage (shown in grey). The crystallographic  $abc$  and octahedral  $xyz$  coordinates are shown. The  $x, y, z$  bonds are colored green, blue, and red respectively. (b) Single-ion level scheme for the  $J = 2$  moment. The fivefold degeneracy is split by an energy gap  $\Delta$  into a low-lying non-Kramers  $E_g$  doublet and an excited  $T_{2g}$  triplet by electronic  $t_{2g}$ - $e_g$  mixing induced by spin-orbit coupling [32, 34]. The  $E_g$  and  $T_{2g}$  states are also shown where red and blue represent non-zero spin density.

cal phase diagram. Noticing a special point in the phase diagram which maps to the pure antiferro-Kitaev model, we investigate the extent of the KML in the quantum phase diagram using exact diagonalization (ED) on the 24-site cluster. We summarize our results and discuss the conditions to realize signatures of the KML in  $5d^2$  honeycomb insulators.

*Multipolar pseudospin-1/2 interactions*—Electronic states of transition metal ions enclosed in an octahedral cage are generally split by cubic crystal fields into a low-lying  $t_{2g}$  triplet and an excited  $e_g$  doublet. For a  $d^2$  filling, the orbital sector is described by three antisymmetrized two-electron states, forming an effective total angular momentum  $L = 1$  which is then coupled to the total spin  $S = 1$  via spin-orbit coupling, resulting in the  $J = 2$  multiplet [38]. The  $J = 2$  dipole operators are given by  $J_\gamma = \hat{e}_\gamma \cdot \mathbf{J}$  for  $\gamma \in \{x, y, z\}$ , where  $\hat{e}_{x,y,z}$  point along the three anion directions, see Fig. 1(a). The fivefold-degenerate  $J = 2$  state can then be

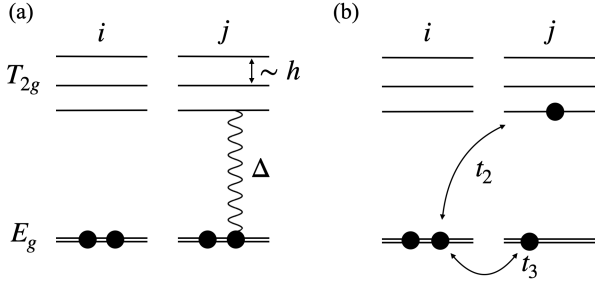


Figure 2. A schematic of a virtual process that contributes to both  $J_B$  and  $h_{\text{eff}}$  term in the effective Hamiltonian Eq. (2) at third order for the case of a magnetic field aligned along the  $c$ -axis. The  $E_g$  and  $T_{2g}$  states at site  $j$  mix due to (a) the on-site Zeeman field, and (b) hopping of an electron via interorbital  $t_2$  and intraorbital  $t_3$ , see visual representation of the orbital overlaps in Fig. 1 of the SM [39]. The overall contribution is then proportional to  $(t_2 t_3 / U)(h / \Delta)$ .

further split by virtual processes mixing the electronic  $t_{2g}$  and  $e_g$  states via spin-orbital excitations, resulting in a ground state doublet and excited triplet separated by energy gap  $\Delta$ , see Fig. 1(b). In analogy with the five electronic  $d$  orbital states, we refer to the doublet and triplet states as  $E_g$  and  $T_{2g}$  respectively. The  $E_g$  doublet is of the non-Kramers type with vanishing magnetic dipole moment, but carries higher-rank moments i.e., quadrupole and octupole moments denoted by the operators  $Q_{x^2-y^2} = J_x^2 - J_y^2$ ,  $Q_{3z^2} = (3J_z^2 - \mathbf{J}^2) / \sqrt{3}$ , and  $T_{xyz} = \frac{\sqrt{15}}{6} \overline{J_x J_y J_z}$ , where the overline symbol denotes symmetrization of the underlying operators. Let us define three operators  $s^{a,b,c}$  as

$$(s^a, s^b, s^c) \equiv \frac{1}{2} \mathcal{P}_{E_g}^\dagger \left( \frac{Q_{3z^2}}{2\sqrt{3}}, \frac{Q_{x^2-y^2}}{2\sqrt{3}}, \frac{T_{xyz}}{3\sqrt{5}} \right) \mathcal{P}_{E_g}, \quad (1)$$

where  $\mathcal{P}_{E_g}$  is the projection operator onto the  $E_g$  doublet. The action of these operators on the  $E_g$  subspace can be represented by the three Pauli matrices  $(s^a, s^b, s^c) = (\sigma^3, \sigma^1, \sigma^2) / 2$ , so that  $s^{a,b,c}$  form effective pseudospin-1/2 operators. The components are given by  $s^{\tilde{\gamma}} = \hat{\mathbf{e}}_{\tilde{\gamma}} \cdot \mathbf{s}$  for  $\tilde{\gamma} \in \{a, b, c\}$ , where  $\hat{\mathbf{e}}_c$  points out of the honeycomb plane spanned by  $\hat{\mathbf{e}}_a$  and  $\hat{\mathbf{e}}_b$ , see Fig. 1(a). The quadrupolar and octupolar moments are in one-to-one correspondence with the projection of  $\mathbf{s}$  onto the  $ab$ -plane or the  $c$ -axis, respectively.

We now investigate the form of the multipolar interactions by introducing  $t_{2g}$  orbital hopping, as was done in the case of the  $d^2$  double perovskites [35–37]. On a honeycomb  $z$ -bond, the parameters  $t_3$  and  $t_1$  represent intraorbital hopping through  $xy - xy$  overlap, or  $xz - xz$  and  $yz - yz$  overlaps, respectively; see Fig. 1 of the Supplemental Material (SM) [39]. We also introduce an  $xz - yz$  interorbital hopping through the edge-shared anions by hopping parameter  $t_2$ . We go beyond earlier studies by immersing the system in an external magnetic field  $\mathbf{h} = (h^x, h^y, h^z)$ . The spin and orbital

degrees of freedom are sensitive to this field via a Zeeman coupling  $H^Z = \mu_B (\mathbf{L} + 2\mathbf{S}) \cdot \mathbf{h} = g_J \mu_B \mathbf{J} \cdot \mathbf{h}$ , which introduces off-diagonal matrix elements between the doublet and triplet states [39]. We ensure that the  $E_g$  and  $T_{2g}$  manifolds remain well-separated by considering the low-field limit  $g_J \mu_B |\mathbf{h}| \ll \Delta$  so that the perturbative expansion is carried out in both  $|\mathbf{h}| / \Delta$  and  $t_{ij}^2 / U$ , where  $t_{ij}$  is some hopping between sites  $i$  and  $j$  and  $U$  is the Hubbard energy cost of double-occupancy. The external field gives rise to new virtual processes where the  $E_g$  doublet mixes with the polarized  $T_{2g}$  triplet during the hopping procedure, see Fig. 2. This process generates new terms in the effective Hamiltonian denoted by  $J_B^\gamma$  and  $\mathbf{h}_{\text{eff}} = (h_{\text{eff}}^a, h_{\text{eff}}^b, h_{\text{eff}}^c)$  appearing at third order in addition to the previously derived  $J_\tau, J_Q$ , and  $J_O$ :

$$H = \sum_{\langle ij \rangle_\gamma} J_\tau \tau_i^\gamma \tau_j^\gamma + J_Q (s_i^a s_j^a + s_i^b s_j^b) + J_O s_i^c s_j^c - \sqrt{2} J_B^\gamma (\tau_i^\gamma s_j^c + s_i^c \tau_j^\gamma) - \sum_i \mathbf{h}_{\text{eff}} \cdot \mathbf{s}_i, \quad (2)$$

where  $\tau^\gamma \equiv s^a \cos \phi_\gamma + s^b \sin \phi_\gamma$  is a compass quadrupole operator with  $\phi_\gamma = 0, 2\pi/3, 4\pi/3$  for a given bond of type  $\gamma = z, x, y$ . Crucially, the addition of a magnetic field supplements the Hamiltonian of Ref. [37] with terms ordinarily forbidden by time-reversal symmetry, including a bond-anisotropic quadrupole-octupole interaction  $J_B^\gamma$ , that is,  $J_B^x, J_B^y$ , and  $J_B^z$  generally differ in strength along each bond. For the case of a [111] magnetic field  $\mathbf{h} = h \hat{\mathbf{e}}_c$ , the  $J_B^\gamma$  interaction becomes bond-isotropic with  $J_B \equiv J_B^x = J_B^y = J_B^z = J_B$ , and  $h_{\text{eff}}^a = h_{\text{eff}}^b = 0, h_{\text{eff}}^c \equiv h_{\text{eff}}$ , where

$$J_B = \frac{8 t_2 (2t_1 + t_3) g_J \mu_B h}{9 U \Delta} j_x^{\uparrow-},$$

$$h_{\text{eff}} = \frac{2 t_2 (t_1 - t_3) g_J \mu_B h}{3 U \Delta} j_z^{\uparrow 0} - 24 \frac{(g_J \mu_B h)^3}{\Delta^2} j_x^{\uparrow+} j_z^{\uparrow+} j_x^{\uparrow+}, \quad (3)$$

where  $j_\alpha^{\mu\nu} \equiv \langle \mu | J_\alpha | \nu \rangle$ ,  $|\uparrow\rangle$  is one of the  $E_g$  states and  $\{|\pm\rangle, |0\rangle\}$  are the three  $T_{2g}$  states [39]. For the remainder of this Letter we focus on the case of a [111] magnetic field; the general form of  $J_B^\gamma$  and  $\mathbf{h}_{\text{eff}}$  for an arbitrary magnetic field direction are given in Section II of the SM [39], along with the expressions for  $J_\tau, J_Q$ , and  $J_O$  previously derived in Ref. [37].

*Classical phase diagrams*—We now explore the phase diagram of the  $J_\tau - J_Q - J_O - J_B - h_{\text{eff}}$  model. We study the phase diagram of the Hamiltonian Eq. (2) in the classical limit by treating  $\mathbf{s}$  as an  $O(3)$  vector using Monte Carlo simulated annealing to obtain the classical ground states [40–42]; see Appendix A of Ref. [43] for simulation details. Signatures of quadrupolar and octupolar ordering are given by peaks in the structure factors  $\frac{1}{N} \sum_{ij} (s_i^a s_j^a + s_i^b s_j^b) e^{-i\mathbf{q} \cdot (\mathbf{r}_i - \mathbf{r}_j)}$  and  $\frac{1}{N} \sum_{ij} s_i^c s_j^c e^{-i\mathbf{q} \cdot (\mathbf{r}_i - \mathbf{r}_j)}$ , respectively. We focus on

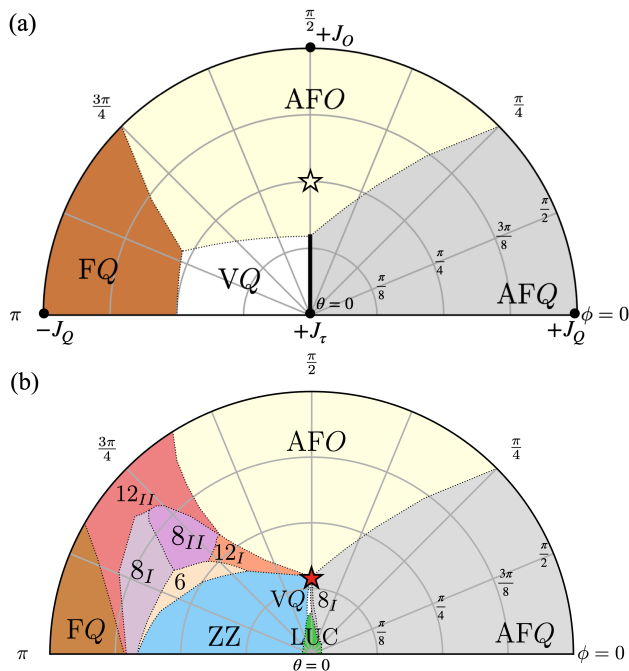


Figure 3. Classical phase diagrams computed by Monte Carlo simulated annealing at  $h_{\text{eff}} = 0$  and (a)  $J_B = 0$ , and (b)  $J_B = \bar{J}/\sqrt{5}$ , where  $\bar{J} = 1$  sets the energy scale. The angles  $(\theta, \phi)$  parameterize the exchange interactions in Eq. (2) as  $J_\tau = \bar{J} \cos \theta$ ,  $J_Q = \bar{J} \sin \theta \cos \phi$ ,  $J_O = \bar{J} \sin \theta \sin \phi$ . Some phases are labelled by the number of sites in the ordering unit cell; two such phases with identical unit cell size are distinguished using Roman numerals. In Section III of the SM we display the pseudospin configuration in each ordered phase [39]. The yellow and red stars indicate points shown in Fig. 4; at the red star the Hamiltonian is equivalent to the pure antiferro-Kitaev model.

the region where both  $J_\tau, J_O > 0$  by setting  $J_\tau = \bar{J} \cos \theta$ ,  $J_Q = \bar{J} \sin \theta \cos \phi$ ,  $J_O = \bar{J} \sin \theta \sin \phi$  and restricting to  $0 \leq \theta \leq \pi/2$ ,  $0 \leq \phi \leq \pi$ ; for  $J_B = 0$  the Hamiltonian is invariant under  $\phi \rightarrow 2\pi - \phi$  (i.e.  $J_O \rightarrow -J_O$ ) and  $s^c \rightarrow -s^c$  on one of the two honeycomb sublattices. In Fig. 3(a) we present the phase diagram at fixed  $J_B = h_{\text{eff}} = 0$  which is dominated by the antiferro-octupole (AFO), antiferro-quadrupole (AFQ), ferro-quadrupole (FQ), and vortex-quadrupole (VQ) phases; the VQ phase in particular is a six-site quadrupolar phase, see Section III of the SM for pseudospin configuration [39]. Note that each of these phases host either quadrupolar or octupolar moments, but not both. The line where  $J_Q = 0$  and  $0 \leq J_O \leq J_\tau/2$  hosts a *disordered* quadrupolar state originating from the pure  $J_\tau$  limit at  $\theta = 0$ . There the model has a macroscopically large ground state manifold owing to the physics of the  $120^\circ$  compass honeycomb model [7, 44, 45]. The octupolar Ising interaction, which is proportional to  $s_i^c s_j^c$ , does not immediately lift this degeneracy until  $J_O > J_\tau/2$  where the AFO phase is stabilized in a spin-flop transition. On the other hand, the degeneracy is lifted by finite

$J_Q$  and selects either VQ or AFQ ordering depending on the sign of  $J_Q$ .

In Fig. 3(b) we present the classical phase diagram at a fixed value of  $J_B = \bar{J}/\sqrt{5} > 0$ , which modifies the  $J_B = 0$  case in several notable ways. Firstly, the area surrounding the disordered quadrupolar state in the  $J_B = 0$  limit now hosts several large unit cell (LUC) orders including 24-site and 40-site orders. Secondly, whereas the region where both  $J_Q, J_O > 0$  is relatively undisturbed, the opposite limit where  $J_Q$  and  $J_O$  differ by a sign hosts a variety of new ordered phases. An example is the zigzag (ZZ) phase which contains both an in-plane and out-of-plane component, see Fig. 4. In fact, all new phases appearing in Fig. 3(b) feature both quadrupolar and octupolar moments, see Section III of the SM for a visual representation of the classical pseudospin moments [39]. Thirdly, six different phases emerge from a single point indicated by a red star in Fig. 3(b). In the next section we explore this point in detail and consider the consequences for the quantum pseudospin model.

*Kitaev multipolar liquid*—To find the relation to the Kitaev model, we rewrite the Hamiltonian Eq. (2) in the octahedral  $xyz$  coordinates, where it may be written in the  $JK\Gamma\Gamma'$  form:

$$H = \sum_{\langle ij \rangle_\gamma} J \mathbf{s}_i \cdot \mathbf{s}_j + K s_i^\gamma s_j^\gamma + \Gamma (s_i^\alpha s_j^\beta + s_i^\beta s_j^\alpha) \quad (4)$$

$$+ \Gamma' [s_i^\gamma s_j^\alpha + s_i^\alpha s_j^\gamma + (\alpha \rightarrow \beta)] - h_{\text{eff}} \sum_i \hat{\mathbf{e}}_c \cdot \mathbf{s}_i$$

where  $s^\gamma = \hat{\mathbf{e}}_\gamma \cdot \mathbf{s}$ ,  $\gamma \in \{x, y, z\}$ , and  $\alpha, \beta \in \{x, y, z\} \setminus \{\gamma\}$ . The values of  $J, K, \Gamma$  and  $\Gamma'$  are given by

$$J = \frac{1}{3} \left( \frac{1}{2} J_\tau - 2J_B + J_O + 2J_Q \right),$$

$$K = \frac{1}{2} J_\tau + 2J_B, \quad \Gamma = J - J_Q, \quad (5)$$

$$\Gamma' = \frac{1}{3} (-J_\tau + J_B + J_O - J_Q).$$

The special point indicated by the red star in Fig. 3(b) is where  $J_Q = h_{\text{eff}} = 0$  and the other parameters satisfy the ratio  $J_\tau : J_O : J_B = 2 : 1 : 1$ . Here the Hamiltonian takes the form  $H = \sum_{\langle ij \rangle_\gamma} \bar{K} s_i^\gamma s_j^\gamma$  where  $\bar{K} = 3J_\tau/2 > 0$ ; in other words, our multipolar pseudospin model is described purely by an antiferro-Kitaev interaction. The classical limit of this model hosts an extensive ground state degeneracy, which explains why several classical phases meet at the red star in Fig. 3(b). In analogy to the Kitaev honeycomb model for spin-1/2 moments, we can write the multipolar pseudospin operator in terms of Majorana fermions  $b^\gamma$  and  $c$  as  $s^\gamma = ib^\gamma c/2$ , and the model can be solved exactly in terms of Majorana fermions hopping with a Dirac dispersion in the presence of a background  $\mathbb{Z}_2$  gauge field. The resulting entangled ground state lacks long-range multipolar order, which we recognize as the KML. The discovery of an exotic phase

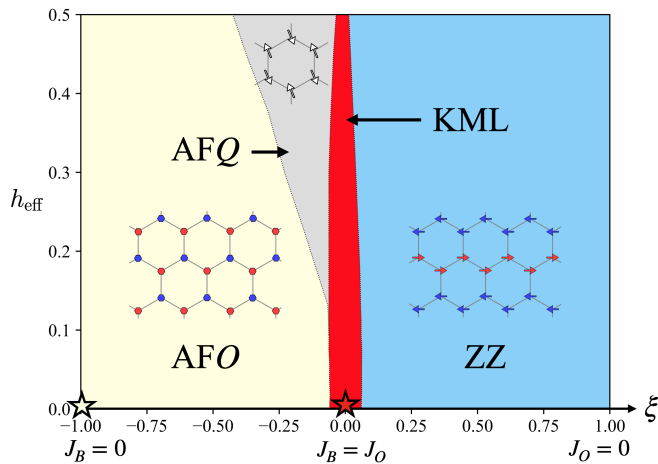


Figure 4. Quantum phase diagram obtained by 24-site ED, where the parameters  $\xi = (J_B - J_O) / (J_B + J_O)$  and  $h_{\text{eff}}$  are tuned while  $J_Q = 0$  and  $J_\tau = J_B + J_O = 1$  are fixed. Phase boundaries are given by peaks in the ground state energy derivatives, and we determine the presence and type of ordering by calculating the quadrupolar and octupolar structure factors of each phase shown in Section III of the SM [39]. The yellow star in corresponds to the point where  $J_\tau = J_O$  whereas the red star corresponds to the antiferro-Kitaev point. For each ordered phase, the arrows represent each pseudospin's in-plane (i.e. quadrupolar) component, whereas red and blue colors indicates the out-of-plane (i.e. octupolar) component with opposite directions.

in an exactly-solvable model of multipolar moments in  $d^2$  honeycomb materials forms the central result of this Letter.

We would like to find the ordered multipole phases nearby the KML phase space as  $J_B$  and  $h_{\text{eff}}$  are tuned, as the KML physics may govern the finite temperature above which the multipole ordering melts. To do so, we solve Eq. (2) using ED on the 24-site cluster with the numerical package  $\mathcal{H}\Phi$  [46]. We parameterize the quantum phase diagram by fixing  $J_Q = 0$  and tuning the parameter  $\xi = (J_B - J_O) / (J_B + J_O)$  between  $\xi \in [-1, 1]$ . Whereas  $\xi = -1$  corresponds to the point where  $J_B = 0$  and  $J_\tau = J_O$ , shown in Fig. 3(a) by the yellow star,  $\xi = 0$  corresponds to the point where  $J_B = J_O = J_\tau/2$  which maps to the pure antiferro-Kitaev point. The three ordered phases AFO, AFQ, and ZZ dominate the phase diagram. However, there exists a narrow window where the KML is stabilized which is extended in the  $h_{\text{eff}}$  direction until roughly  $h_{\text{eff}} \sim 0.6 J_\tau$ . At the antiferro-Kitaev point, the KML is not immediately susceptible to polarization as the ferro-octupole configuration does not lie within the antiferro-Kitaev ground state manifold.

One may expect that, due to the relations implied by Eq. (5), other ordered phases explored in the  $JKTT'$  literature can be stabilized by the model Eq. (2) including the four-site stripy phase. Yet this phase does not appear in our work, as it primarily occupies the  $K < 0$

region [4, 6] and we have focused on the region where  $J_\tau, J_B \geq 0$ , i.e.  $K \geq 0$ . A small stripy phase could appear near  $K > 0$  when  $\Gamma < 0$  and  $\Gamma' > 0$  [25] but it lies outside our parameter space.

*Discussion and summary*—We now discuss the conditions to realize the KML in  $5d^2$  insulators. The bond-dependent quadrupole-octupole interaction requires the Zeeman field which induces off-diagonal components between the  $E_g$  and  $T_{2g}$  states while maintaining their energy separation  $\Delta$ ; thus the first condition is that  $g_J \mu_B h \ll \Delta$ . In the  $\text{Os}^{6+}$  and  $\text{Re}^{5+}$  double perovskites  $\Delta$  is around 10-20 meV, restricting  $h \sim \mathcal{O}(10 \text{ T})$ . The second condition is approaching the Kitaev limit. In most edge-sharing materials,  $|t_2|, |t_3| \gg |t_1|$  [6] so that the Kitaev limit is best approached if  $t_2^2 \sim 2t_1t_3$ , since  $J_Q \sim 0$  and  $J_O \sim 4t_2^2/3$  while  $J_\tau \sim 4t_3^2/9$ , see expressions given in Section I of the SM [39]. The ratio of  $t_2$  and  $t_3$  then determines whether the material is VQ-, AFQ-, or AFO-ordered in the zero-field limit shown in Fig. 3(a). As the magnetic field is introduced and  $J_B$  is increased, the system approaches the KML phase space but it may remain in the ordered phase depending on  $t_2/t_3$ . The signature of KML physics is then revealed at the finite temperatures above which the ordering vanishes. The intricate balance between the field strength  $h/\Delta$  and exchange paths presents a challenge for the material realization of the KML. Nevertheless, this work serves as a “proof-of-concept” that the  $d^2$  spin-orbit entangled honeycomb insulators with non-Kramers doublets may exhibit multipolar Kitaev physics.

In this Letter we have shown that the KML can arise in a spin-orbit coupled  $d^2$  honeycomb material. The key ingredient is the application of a magnetic field which allows for bond-dependent quadrupole-octupole interactions in the effective Hamiltonian of the  $E_g$  doublet. In combination with the Ising octupole and  $120^\circ$  compass-like quadrupole terms, the Hamiltonian can be tuned to the pure Kitaev form. The resulting multipolar model can then be solved exactly using Majorana fermions, in analogy with Kitaev's original spin-1/2 model. Multipolar ordered phases arise along with the KML, including those featuring combinations of quadrupolar and octupolar ordering, as well as a disordered compass-quadrupole phase. The nature and extent of these phases in the quantum phase diagram form interesting avenues of future work. We have also shown that the field-induced bond-dependent  $J_B$  becomes bond-anisotropic when the field is tilted away from the  $c$ -axis. This extended phase space, and the novel physics contained within, motivates future studies of  $d^2$  multipolar systems.

*Acknowledgements*—A.R. thanks P. P. Stavropoulos, S. Voleti, and F. D. Wandler for helpful discussions. We acknowledge support from the NSERC Discovery Grant No. 2022-04601. H.Y.K also acknowledges support from CIFAR and the Canada Research Chairs Program. Computations were performed on the Niagara supercomputer

at the SciNet HPC Consortium. SciNet is funded by: the Canada Foundation for Innovation under the auspices of Compute Canada; the Government of Ontario; Ontario Research Fund - Research Excellence; and the University of Toronto.

---

\* hykee@physics.utoronto.ca

- [1] A. Y. Kitaev, *Ann. Phys. (NY)* **303**, 2 (2003).
- [2] A. Kitaev, *Ann. Phys. (NY)* **321**, 2 (2006).
- [3] G. Jackeli and G. Khaliullin, *Phys. Rev. Lett.* **102**, 017205 (2009).
- [4] J. Chaloupka, G. Jackeli, and G. Khaliullin, *Phys. Rev. Lett.* **105**, 027204 (2010).
- [5] W. Witczak-Krempa, G. Chen, Y. B. Kim, and L. Balents, *Annual Review of Condensed Matter Physics* **5**, 57 (2014).
- [6] J. G. Rau, E. K.-H. Lee, and H.-Y. Kee, *Phys. Rev. Lett.* **112**, 077204 (2014).
- [7] Z. Nussinov and J. van den Brink, *Rev. Mod. Phys.* **87**, 1 (2015).
- [8] J. G. Rau, E. K.-H. Lee, and H.-Y. Kee, *Annual Review of Condensed Matter Physics* **7**, 195 (2016).
- [9] S. M. Winter, A. A. Tsirlin, M. Daghofer, J. van den Brink, Y. Singh, P. Gegenwart, and R. Valentí, *J. Phys.: Condens. Matter* **29**, 493002 (2017).
- [10] Y. Motome, R. Sano, S. Jang, Y. Sugita, and Y. Kato, *Journal of Physics: Condensed Matter* **32**, 404001 (2020).
- [11] T. Takayama, J. Chaloupka, A. Smerald, G. Khaliullin, and H. Takagi, *Journal of the Physical Society of Japan* **90**, 062001 (2021).
- [12] S. Trebst and C. Hickey, *Physics Reports* **950**, 1 (2022).
- [13] K. W. Plumb, J. P. Clancy, L. J. Sandilands, V. V. Shankar, Y. F. Hu, K. S. Burch, H.-Y. Kee, and Y.-J. Kim, *Phys. Rev. B* **90**, 041112(R) (2014).
- [14] H.-S. Kim, Vijay Shankar V., A. Catuneanu, and H.-Y. Kee, *Phys. Rev. B* **91**, 241110(R) (2015).
- [15] A. Koitzsch, C. Habenicht, E. Müller, M. Knupfer, B. Büchner, H. C. Kandpal, J. van den Brink, D. Nowak, A. Isaeva, and T. Doert, *Phys. Rev. Lett.* **117**, 126403 (2016).
- [16] L. J. Sandilands, Y. Tian, A. A. Reijnders, H.-S. Kim, K. W. Plumb, Y.-J. Kim, H.-Y. Kee, and K. S. Burch, *Phys. Rev. B* **93**, 075144 (2016).
- [17] X. Zhou, H. Li, J. A. Waugh, S. Parham, H.-S. Kim, J. A. Sears, A. Gomes, H.-Y. Kee, Y.-J. Kim, and D. S. Dessau, *Phys. Rev. B* **94**, 161106(R) (2016).
- [18] A. Banerjee, C. A. Bridges, J.-Q. Yan, A. A. Aczel, L. Li, M. B. Stone, G. E. Granroth, M. D. Lumsden, Y. Yiu, J. Knolle, S. Bhattacharjee, D. L. Kovrizhin, R. Moessner, D. A. Tennant, D. G. Mandrus, and S. E. Nagler, *Nat. Mater.* **15**, 733 (2016).
- [19] H.-S. Kim and H.-Y. Kee, *Phys. Rev. B* **93**, 155143 (2016).
- [20] S. M. Winter, Y. Li, H. O. Jeschke, and R. Valentí, *Phys. Rev. B* **93**, 214431 (2016).
- [21] L. Janssen, E. C. Andrade, and M. Vojta, *Phys. Rev. B* **96**, 064430 (2017).
- [22] W. Wang, Z.-Y. Dong, S.-L. Yu, and J.-X. Li, *Phys. Rev. B* **96**, 115103 (2017).
- [23] P. Laurell and S. Okamoto, *npj Quantum Mater.* **5**, 2 (2020).
- [24] Y. Singh, S. Manni, J. Reuther, T. Berlijn, R. Thomale, W. Ku, S. Trebst, and P. Gegenwart, *Phys. Rev. Lett.* **108**, 127203 (2012).
- [25] J. G. Rau and H.-Y. Kee, arXiv:1408.4811.
- [26] S. Hwan Chun, J.-W. Kim, J. Kim, H. Zheng, C. Stoumpos, C. Malliakas, J. Mitchell, K. Mehlawat, Y. Singh, Y. Choi, T. Gog, A. Al-Zein, M. Sala, M. Krisch, J. Chaloupka, G. Jackeli, G. Khaliullin, and B. J. Kim, *Nature Physics* **11**, 462 (2015).
- [27] S. C. Williams, R. D. Johnson, F. Freund, S. Choi, A. Jesche, I. Kimchi, S. Manni, A. Bombardi, P. Manuel, P. Gegenwart, and R. Coldea, *Phys. Rev. B* **93**, 195158 (2016).
- [28] H. Liu and G. Khaliullin, *Phys. Rev. B* **97**, 014407 (2018).
- [29] R. Sano, Y. Kato, and Y. Motome, *Phys. Rev. B* **97**, 014408 (2018).
- [30] H. Liu, J. Chaloupka, and G. Khaliullin, *Phys. Rev. Lett.* **125**, 047201 (2020).
- [31] M. Songvilay, J. Robert, S. Petit, J. A. Rodriguez-Rivera, W. D. Ratcliff, F. Damay, V. Balédent, M. Jiménez-Ruiz, P. Lejay, E. Pachoud, A. Hadj-Azzem, V. Simonet, and C. Stock, *Phys. Rev. B* **102**, 224429 (2020).
- [32] A. Paramekanti, D. D. Maharaj, and B. D. Gaulin, *Phys. Rev. B* **101**, 054439 (2020).
- [33] D. D. Maharaj, G. Sala, M. B. Stone, E. Kermarrec, C. Ritter, F. Fauth, C. A. Marjerrison, J. E. Greedan, A. Paramekanti, and B. D. Gaulin, *Phys. Rev. Lett.* **124**, 087206 (2020).
- [34] S. Voleti, D. D. Maharaj, B. D. Gaulin, G. Luke, and A. Paramekanti, *Phys. Rev. B* **101**, 155118 (2020).
- [35] G. Khaliullin, D. Churchill, P. P. Stavropoulos, and H.-Y. Kee, *Phys. Rev. Research* **3**, 033163 (2021).
- [36] S. Voleti, A. Haldar, and A. Paramekanti, *Phys. Rev. B* **104**, 174431 (2021).
- [37] D. Churchill and H.-Y. Kee, *Phys. Rev. B* **105**, 014438 (2022).
- [38] G. Chen and L. Balents, *Phys. Rev. B* **84**, 094420 (2011).
- [39] See Supplemental Material at <http://link.aps.org/supplemental/10.1103/PhysRevB.107.L020408> for the derivation of the effective pseudospin Hamiltonian for arbitrary magnetic field directions, the definition of the  $E_g/T_{2g}$  states, and the representation of the Zeeman field in this basis. It also includes pseudospin configurations obtained by classical Monte Carlo as well as structure factors obtained by 24-site exact diagonalization.
- [40] N. Metropolis, A. W. Rosenbluth, M. N. Rosenbluth, A. H. Teller, and E. Teller, *The Journal of Chemical Physics* **21**, 1087 (1953).
- [41] S. Kirkpatrick, C. D. Gelatt, and M. P. Vecchi, *Science* **220**, 671 (1983).
- [42] S. Kirkpatrick, *Journal of Statistical Physics* **34**, 975 (1984).
- [43] A. Rayyan, Q. Luo, and H.-Y. Kee, *Phys. Rev. B* **104**, 094431 (2021).
- [44] C. Wu, *Phys. Rev. Lett.* **100**, 200406 (2008).
- [45] J. Nasu, A. Nagano, M. Naka, and S. Ishihara, *Phys. Rev. B* **78**, 024416 (2008).
- [46] M. Kawamura, K. Yoshimi, T. Misawa, Y. Yamaji, S. Todo, and N. Kawashima, *Computer Physics Communications* **217**, 180 (2017).

Supplemental material for “Field-induced Kitaev multipolar liquid  
in spin-orbit coupled  $d^2$  honeycomb Mott insulators”

Ahmed Rayyan,<sup>1</sup> Derek Churchill,<sup>1</sup> and Hae-Young Kee<sup>1,2,\*</sup>

<sup>1</sup>*Department of Physics, University of Toronto, Toronto ON M5S 1A7, Canada*

<sup>2</sup>*CIFAR Program in Quantum Materials,*

*Canadian Institute for Advanced Research, Toronto ON M5G 1M1, Canada*

(Dated: March 8, 2023)

arXiv:2206.10647v2 [cond-mat.str-el] 7 Mar 2023

## I. DERIVATION OF THE EFFECTIVE $E_g$ HAMILTONIAN

In this section we outline how the effective  $E_g$  pseudospin model is obtained. We consider the limit where the octahedral crystal field splitting and electron-electron repulsion are the dominant interactions, justifying a strong-coupling approach where the  $d^2$  electrons lie in the  $t_{2g}$  manifold and form a degenerate ground state that is lifted by the electron hopping and magnetic field. Let us introduce the creation operator  $c_{m\sigma}^\dagger$  which creates a  $t_{2g}$  electron with spin and orbital states denoted by  $\sigma \in \{+, -\}$  and  $m \in \{xy, xz, yz\}$ , respectively. Our starting point is the on-site Kanamori-Hubbard Hamiltonian on a single site  $i$  which is given by

$$\begin{aligned}
H^{\text{KH}} = & U \sum_m n_{m+} n_{m-} + U' \sum_{m \neq m'} n_{m+} n_{m'-} + (U' - J_H) \sum_{m < m', \sigma} n_{m\sigma} n_{m'\sigma} \\
& + J_H \sum_{m \neq m'} \left( c_{m+}^\dagger c_{m'-}^\dagger c_{m-} c_{m'+} + c_{m+}^\dagger c_{m-}^\dagger c_{m'-} c_{m'+} \right) - \lambda \mathbf{L} \cdot \mathbf{S}
\end{aligned} \tag{1}$$

where  $n_{m\sigma} = c_{m\sigma}^\dagger c_{m\sigma}$  is the number operator, and  $\mathbf{L} = \mathbf{l}_1 + \mathbf{l}_2$  and  $\mathbf{S} = \mathbf{s}_1 + \mathbf{s}_2$  are the total orbital and spin angular momentum operators, respectively. The parameters  $U$  and  $U' = U - 2J_H$  are intraorbital and interorbital Coulomb interactions respectively, where  $J_H$  is the Hund's coupling. Lastly, the spin-orbit coupling parameter  $\lambda$  is related to the single particle spin-orbit coupling  $\zeta (\mathbf{l}_1 \cdot \mathbf{s}_1 + \mathbf{l}_2 \cdot \mathbf{s}_2)$  via  $\lambda = \zeta/n$  where  $n = 2$  is the electron filling. For the  $d^2$  filling, the limit  $10Dq, U > \zeta, J_H$  leads to a fivefold  $J = 2$  manifold that is further split into an  $E_g$  doublet and  $T_{2g}$  triplet (see Section II of Supplemental Material) by spin-orbit-coupling induced  $t_{2g} - e_g$  mixing with energy gap  $\Delta \sim \zeta^2/10Dq$  [1, 2].

Now let us consider two honeycomb sites labelled  $i = 1, 2$  connected by a  $z$ -bond such that their octahedra share one edge. In the isolated limit the Hamiltonian is given by  $H_1^{\text{KH}} + H_2^{\text{KH}}$  with a ground state  $E_g$  doublet on both sites. Interactions are introduced by projecting the electron hopping and magnetic field onto the  $E_g$  doublet; in this section we focus on the electron hopping as the case of the magnetic field is studied in the next section. The orbital part of the tight-binding Hamiltonian is given by  $H_{(12)_z}^{\text{TB}} = c_1^\dagger T_{(12)_z} c_2 + c_2^\dagger T_{(12)_z}^\dagger c_1$  where  $c_i^\dagger = (c_{i,yz}^\dagger, c_{i,xz}^\dagger, c_{i,xy}^\dagger)$  and

$$T_{(12)_z} = \begin{pmatrix} t_1 & t_2 & 0 \\ t_2 & t_1 & 0 \\ 0 & 0 & t_3 \end{pmatrix} \tag{2}$$



is fixed by inversion about the  $z$ -bond center and the  $C_2$  symmetry about the  $\hat{\mathbf{e}}_b$  axis for the undistorted octahedra [3]. The hopping parameter  $t_3$  and  $t_1$  correspond to direct intraorbital exchange, whereas  $t_2$  parameterizes the effective interorbital  $xz - yz$  hopping including  $p$ -orbital superexchange. In Fig. 1 we display the types of orbital overlap which lead to the three hopping parameters.

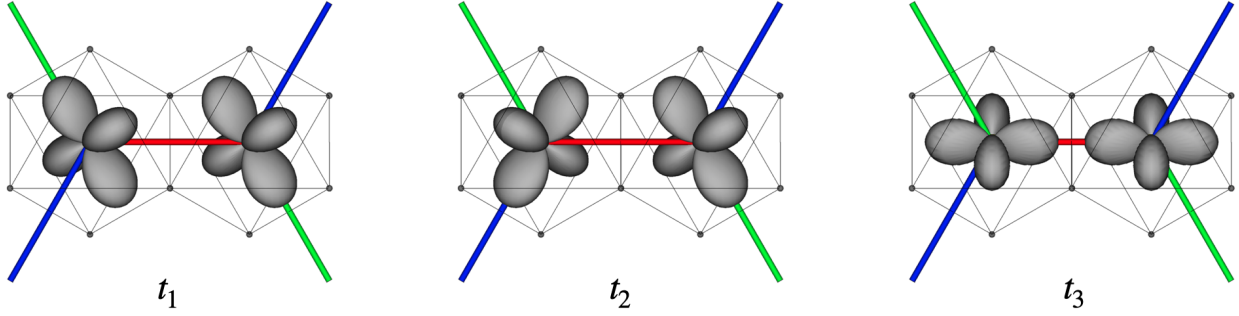


Figure 1. Examples of overlapping orbitals which contribute to the hopping strengths  $t_1, t_2, t_3$  in the  $z$ -bond hopping matrix Eq. (2).

We now carry out the degenerate perturbation theory where the local Kanamori-Hubbard Hamiltonian  $H_0 = H_1^{\text{KH}} + H_2^{\text{KH}}$  is perturbed by  $V = H_{(12)_z}^{\text{TB}} + H_1^Z + H_2^Z$ , ie. the tight-binding Hamiltonian and the on-site Zeeman terms  $H_i^Z = g_J \mu_B \mathbf{J}_i \cdot \mathbf{h}$  (see Section II of Supplemental Material). The perturbative process generates quadratic and linear terms in  $\mathbf{s}_i$  in the effective Hamiltonian. Along the  $z$ -bond, the quadratic terms take on the form

$$H_{(12)_z} = J_\tau s_1^a s_2^a + J_Q (s_1^a s_2^a + s_1^b s_2^b) + J_O s_1^c s_2^c - \sqrt{2} J_B^z (s_1^a s_2^c + s_1^c s_2^a). \quad (3)$$

where  $s^{\bar{\gamma}} = \hat{\mathbf{e}}_{\bar{\gamma}} \cdot \mathbf{s}$  for  $\bar{\gamma} \in \{a, b, c\}$  are the pseudospin-1/2 components in the crystallographic  $abc$  basis given by  $\hat{\mathbf{e}}_a = (\hat{\mathbf{e}}_x + \hat{\mathbf{e}}_y - 2\hat{\mathbf{e}}_z)/\sqrt{6}$ ,  $\hat{\mathbf{e}}_b = (\hat{\mathbf{e}}_y - \hat{\mathbf{e}}_x)/\sqrt{2}$ , and  $\hat{\mathbf{e}}_c = (\hat{\mathbf{e}}_x + \hat{\mathbf{e}}_y + \hat{\mathbf{e}}_z)/\sqrt{3}$ . The field-independent exchange parameters are given by

$$J_\tau = \frac{4(t_1 - t_3)^2}{9U}, \quad J_Q = \frac{2t_1(t_1 + 2t_3) - t_2^2}{3U}, \quad J_O = \frac{2t_1(t_1 + 2t_3) + t_2^2}{3U}, \quad (4)$$

where we set  $J_H$  to zero as it is small relative to  $U$ ; the derivation of  $J_\tau, J_Q$ , and  $J_O$  and the effect of a finite Hund's coupling  $J_H$  was previously studied in Ref. [4]. The field-dependent quadrupole-octupole interaction strength is given by

$$J_B^z = \frac{8}{3\sqrt{6}} \frac{t_2(2t_1 + t_3)}{U} \frac{g_J \mu_B \hbar^z}{\Delta}. \quad (5)$$



The quadratic terms along the  $x$  and  $y$  bonds can be obtained via a  $2\pi/3$  counter-clockwise rotation about the  $[111]$  axis, and the pseudospin transforms accordingly as

$$(s^a, s^b, s^c) \rightarrow \left( -\frac{1}{2}s^a + \frac{\sqrt{3}}{2}s^b, -\frac{\sqrt{3}}{2}s^a - \frac{1}{2}s^b, s^c \right). \quad (6)$$

To simplify notation it is convenient to introduce the compass quadrupole operators given by  $\tau^\gamma \equiv s^a \cos \phi_\gamma + s^b \sin \phi_\gamma$  and  $\bar{\tau}^\gamma \equiv s^b \cos \phi_\gamma - s^a \sin \phi_\gamma$ , where  $\phi_\gamma = 0, 2\pi/3, 4\pi/3$  for a given bond of type  $\gamma = z, x, y$ . The Hamiltonian on each honeycomb bond can then be obtained by sending  $s^a \rightarrow \tau^\gamma$  and  $s^b \rightarrow \bar{\tau}^\gamma$  in Eq. (3). Moreover, the quadrupole-octupole interaction is modified along each bond, namely

$$J_B^x = \frac{8}{3\sqrt{6}} \frac{t_2(2t_1 + t_3)}{U} \frac{g_J \mu_B h^x}{\Delta}, \quad J_B^y = \frac{8}{3\sqrt{6}} \frac{t_2(2t_1 + t_3)}{U} \frac{g_J \mu_B h^y}{\Delta}. \quad (7)$$

The linear term in  $\mathbf{s}_i$  is composed of bond-independent and bond-dependent terms; after summing over the contribution from each bond, the latter terms vanish. The full effective Hamiltonian can then be written as

$$H = \sum_{\langle ij \rangle_\gamma} J_\tau \tau_i^\gamma \tau_j^\gamma + J_Q (s_i^a s_j^a + s_i^b s_j^b) + J_O s_i^c s_j^c - \sqrt{2} J_B^\gamma (\tau_i^\gamma s_j^c + s_i^c \tau_j^\gamma) - \sum_i \mathbf{h}_{\text{eff}} \cdot \mathbf{s}_i, \quad (8)$$

where we used the fact that  $\tau_i^\gamma \tau_j^\gamma + \bar{\tau}_i^\gamma \bar{\tau}_j^\gamma = s_i^a s_j^a + s_i^b s_j^b$  for any bond  $\gamma$ , and  $\mathbf{h}_{\text{eff}} = (h_{\text{eff}}^a, h_{\text{eff}}^b, h_{\text{eff}}^c)$  is expressed in the crystallographic basis  $\hat{\mathbf{e}}_{a,b,c}$  where

$$\begin{aligned} h_{\text{eff}}^a &= 6 (g_J \mu_B)^2 \frac{2h_z^2 - h_x^2 - h_y^2}{\Delta}, \\ h_{\text{eff}}^b &= 6\sqrt{3} (g_J \mu_B)^2 \frac{h_x^2 - h_y^2}{\Delta}, \\ h_{\text{eff}}^c &= \frac{4}{3\sqrt{3}} \frac{t_2(t_1 - t_3)}{U} \frac{g_J \mu_B (h^x + h^y + h^z)}{\Delta} - 36\sqrt{3} (g_J \mu_B)^3 \frac{h_x h_y h_z}{\Delta^2}. \end{aligned} \quad (9)$$

The main text is concerned with the case of a  $[111]$  magnetic field where  $\mathbf{h} = h \hat{\mathbf{e}}_c = \frac{h}{\sqrt{3}} (\hat{\mathbf{e}}_x + \hat{\mathbf{e}}_y + \hat{\mathbf{e}}_z)$ . In this case one finds that  $h_{\text{eff}}^a = h_{\text{eff}}^b = 0$  and  $J_B^x = J_B^y = J_B^z$ , leading to a  $C_3$ -symmetric Hamiltonian. Defining  $j_\alpha^{\mu\nu} = \langle \mu | J_\alpha | \nu \rangle$  where  $\mu, \nu$  label the  $E_g$  and  $T_{2g}$  states given in Section II of the Supplemental Material, the field-dependent parameters are

described by  $J_B \equiv J_B^{x,y,z}$  and  $h_{\text{eff}} \equiv h_{\text{eff}}^c$  given by

$$\begin{aligned}
J_B &= \frac{8}{9\sqrt{2}} \frac{t_2(2t_1+t_3)}{U} \frac{gJ\mu_B h}{\Delta}, \\
&= \frac{8}{9} \frac{t_2(2t_1+t_3)}{U} \frac{gJ\mu_B h}{\Delta} j_x^{\uparrow-}, \\
h_{\text{eff}} &= \frac{4}{3} \frac{t_2(t_1-t_3)}{U} \frac{gJ\mu_B h}{\Delta} - 12 \frac{(gJ\mu_B h)^3}{\Delta^2}, \\
&= \frac{2}{3} \frac{t_2(t_1-t_3)}{U} \frac{gJ\mu_B h}{\Delta} j_z^{\uparrow 0} - 24 \frac{(gJ\mu_B h)^3}{\Delta^2} j_x^{\uparrow+} j_z^{\uparrow+} j_x^{\uparrow+}.
\end{aligned} \tag{10}$$

The Hamiltonian Eq. (8) can be written in a form which more clearly displays its symmetries by expanding the compass quadrupole operators  $\tau_i^\gamma$ , giving

$$\begin{aligned}
H &= \sum_{\langle ij \rangle_\gamma} \left( \frac{J_\tau}{2} + J_Q \right) (s_i^a s_j^a + s_i^b s_j^b) + J_O s_i^c s_j^c \\
&+ \frac{J_\tau}{2} [\cos \phi_\gamma (s_i^a s_j^a - s_i^b s_j^b) - \sin \phi_\gamma (s_i^a s_j^b + s_i^b s_j^a)] \\
&- \sqrt{2} J_B^\gamma [\cos \phi_\gamma (s_i^a s_j^c + s_i^c s_j^a) + \sin \phi_\gamma (s_i^b s_j^c + s_i^c s_j^b)] - \sum_i \mathbf{h}_{\text{eff}} \cdot \mathbf{s}_i.
\end{aligned} \tag{11}$$

It is then straightforward to write the Hamiltonian in the octahedral basis  $\hat{\mathbf{e}}_{x,y,z}$  since the pseudospin components  $s^\gamma = \hat{\mathbf{e}}_\gamma \cdot \mathbf{s}$  for  $\gamma \in \{x, y, z\}$  are given by

$$\begin{pmatrix} s^x \\ s^y \\ s^z \end{pmatrix} = \begin{pmatrix} \frac{1}{\sqrt{6}} & -\frac{1}{\sqrt{2}} & \frac{1}{\sqrt{3}} \\ \frac{1}{\sqrt{6}} & \frac{1}{\sqrt{2}} & \frac{1}{\sqrt{3}} \\ -\frac{2}{\sqrt{6}} & 0 & \frac{1}{\sqrt{3}} \end{pmatrix} \begin{pmatrix} s^a \\ s^b \\ s^c \end{pmatrix}.$$

By performing this rotation one obtains

$$\begin{aligned}
H &= \sum_{\langle ij \rangle_\gamma} J^\gamma \mathbf{s}_i \cdot \mathbf{s}_j + K^\gamma s_i^\gamma s_j^\gamma + \Gamma^\gamma (s_i^\alpha s_j^\beta + s_i^\beta s_j^\alpha) \\
&+ \Gamma'^\gamma [s_i^\gamma s_j^\alpha + s_i^\alpha s_j^\gamma + (\alpha \rightarrow \beta)] - \sum_i \mathbf{h}_{\text{eff}} \cdot \mathbf{s}_i,
\end{aligned} \tag{12}$$

where

$$\begin{aligned}
J^\gamma &= \frac{1}{3} \left( \frac{1}{2} J_\tau - 2J_B^\gamma + J_O + 2J_Q \right), \\
K^\gamma &= \frac{1}{2} J_\tau + 2J_B^\gamma, \quad \Gamma^\gamma = J^\gamma - J_Q, \\
\Gamma'^\gamma &= \frac{1}{3} (-J_\tau + J_B^\gamma + J_O - J_Q).
\end{aligned} \tag{13}$$

For an external field along the  $c$ -axis, the exchange parameters are bond-isotropic, ie.  $K^x = K^y = K^z$  and so on for  $J$ ,  $\Gamma$ , and  $\Gamma'$ .

## II. PROPERTIES OF $J = 2$ STATES UNDER A ZEEMAN FIELD

Here we discuss some details regarding the  $J = 2$  manifold, with angular momentum states satisfying  $J_z |m_J\rangle = m_J |m_J\rangle$  for  $m_J = -2, -1, 0, 1, 2$ . The  $J = 2$  splitting can be modelled by a residual crystal field splitting  $H_\Delta = \Delta (\mathcal{O}_{40} + 5\mathcal{O}_{44})/120$  where  $\Delta > 0$  and

$$\begin{aligned}\mathcal{O}_{40} &= 35J_z^4 - (30J(J+1) - 25)J_z^2 + \text{const.} \\ \mathcal{O}_{44} &= (J_+^4 + J_-^4)/2,\end{aligned}\tag{14}$$

are Stevens operators [1, 2]. The eigenstates of  $H_\Delta$  form a doublet with energy  $E = 0$  and a triplet with  $E = \Delta > 0$ ; these are the  $E_g$  and  $T_{2g}$  states, respectively. We may choose the following basis for the  $E_g$  states

$$|\uparrow\rangle = \frac{1}{\sqrt{2}} (|2\rangle + |-2\rangle), \quad |\downarrow\rangle = |0\rangle,\tag{15}$$

and the  $T_{2g}$  states

$$|\pm\rangle = |\pm 1\rangle, \quad |\bar{0}\rangle = \frac{1}{\sqrt{2}} (|2\rangle - |-2\rangle).\tag{16}$$

Let us denote the projection onto these subspaces as  $\mathcal{P}_{E_g}$  and  $\mathcal{P}_{T_{2g}}$ , respectively. The time-reversal operator acts on the angular momentum states as  $\mathcal{T} |m_J\rangle = (-1)^{m_J} |-m_J\rangle$  and on the angular momentum operator as  $\mathcal{T} \mathbf{J} \mathcal{T}^{-1} = -\mathbf{J}$ . For either  $E_g$  state  $|\sigma\rangle$  where  $\sigma \in \{\uparrow, \downarrow\}$ , time-reversal is equivalent to the identity  $\mathcal{T} |\sigma\rangle = |\sigma\rangle$ . This implies that

$$\begin{aligned}\langle\sigma| \mathbf{J} |\sigma\rangle &= \langle\sigma| \mathcal{T}^{-1} \mathcal{T} \mathbf{J} \mathcal{T}^{-1} \mathcal{T} |\sigma\rangle \\ &= -\langle\sigma| \mathbf{J} |\sigma\rangle,\end{aligned}\tag{17}$$

ie.  $\langle\sigma| \mathbf{J} |\sigma\rangle = 0$ : the  $E_g$  doublet does not carry a dipole moment. In fact it is carried by the  $T_{2g}$  states; the three operators  $l_\gamma = -\mathcal{P}_{T_{2g}}^\dagger J_\gamma \mathcal{P}_{T_{2g}}$  with  $\gamma \in \{x, y, z\}$  form the  $l = 1$  representation of the  $\mathfrak{su}(2)$  algebra.

Now let us add a Zeeman field  $H^Z = \mu_B (\mathbf{L} + 2\mathbf{S}) \cdot \mathbf{h} = g_J \mu_B \mathbf{J} \cdot \mathbf{h}$ , where  $g_J = 1/2$  for  $J = 2$  by the Wigner-Eckart theorem. In the  $\{|\uparrow\rangle, |\downarrow\rangle, |-\rangle, |+\rangle, |\bar{0}\rangle\}$  basis,  $H^Z$  takes the form

$$H^Z = g_J \mu_B \begin{pmatrix} 0 & 0 & \frac{1}{\sqrt{2}} h^+ & \frac{1}{\sqrt{2}} h^- & 2h_z \\ 0 & 0 & \frac{\sqrt{3}}{2} h^- & \frac{\sqrt{3}}{2} h^+ & 0 \\ \frac{1}{\sqrt{2}} h^- & \frac{\sqrt{3}}{2} h^+ & -h_z & 0 & -\frac{1}{\sqrt{2}} h^- \\ \frac{1}{\sqrt{2}} h^+ & \frac{\sqrt{3}}{2} h^- & 0 & h_z & \frac{1}{\sqrt{2}} h^+ \\ 2h_z & 0 & -\frac{1}{\sqrt{2}} h^+ & \frac{1}{\sqrt{2}} h^- & 0 \end{pmatrix}.\tag{18}$$

where  $\mathbf{h} = (h_x, h_y, h_z)$  is expressed in the octahedral basis  $\hat{\mathbf{e}}_{x,y,z}$ , and  $h^\pm = h_x \pm i h_y$ . Note that the Zeeman field leads to a finite off-diagonal block connecting the  $E_g$  and  $T_{2g}$  manifolds. To understand how the  $E_g$  doublet are perturbed by a [111] magnetic field  $\mathbf{h} = h \hat{\mathbf{e}}_c$  we solve the Hamiltonian  $H_\Delta + H_Z$  in the limit where  $\epsilon \equiv g_J \mu_B h / \Delta \ll 1$  using the method of resolvents [5]; the modified  $E_g$  states are given by (neglecting normalization constants)

$$\begin{aligned} |\tilde{\uparrow}\rangle &= |\uparrow\rangle - \frac{\epsilon}{\sqrt{3}} (e^{-i\pi/4} |-\rangle + e^{i\pi/4} |+\rangle + 2|\bar{0}\rangle) + \mathcal{O}(\epsilon^2) \\ |\tilde{\downarrow}\rangle &= |\downarrow\rangle - \epsilon (e^{i\pi/4} |-\rangle + e^{-i\pi/4} |+\rangle) + \mathcal{O}(\epsilon^2) \end{aligned} \quad (19)$$

with the field lowering the energy of both states to  $E = -2\epsilon^2 + \mathcal{O}(\epsilon^3)$ .

### III. PROPERTIES OF MULTIPOLAR ORDERS

In this section we discuss some properties of the multipolar phases found in the phase diagrams of the main text.

#### A. Phases in the classical model

Let us recall that the classical phase diagrams in Fig. 3 of the main text are parameterized by  $(\theta, \phi, J_B)$ , where  $J_\tau = \bar{J} \cos \theta$ ,  $J_Q = \bar{J} \sin \theta \cos \phi$ , and  $J_O = \bar{J} \sin \theta \sin \phi$  at fixed  $h_{\text{eff}} = 0$  and either  $J_B = 0$  or  $\bar{J}/\sqrt{5}$  for Fig. 3(a) or 3(b), respectively. In the classical limit, each pseudospin  $\mathbf{s}_i = s_i^a \hat{\mathbf{e}}_a + s_i^b \hat{\mathbf{e}}_b + s_i^c \hat{\mathbf{e}}_c$  is then treated as an  $O(3)$  vector satisfying  $|\mathbf{s}_i \cdot \mathbf{s}_i| = 1$ ; the ground state can then be obtained by Monte Carlo simulated annealing [6–8], see Appendix A of Ref. [9] for simulation details. For a given pseudospin  $\mathbf{s}_i$ , Eq. (1) of the main text suggests that a finite in-plane component  $s_i^a \hat{\mathbf{e}}_a + s_i^b \hat{\mathbf{e}}_b$  corresponds to quadrupolar moments whereas a finite out-of-plane component  $s_i^c$  corresponds to the octupolar moment. In Figs. 2-13 we present pseudospin configurations of each ordered phase that appears in Fig. 3 of the main text along with the ordered unit cell. The size of each arrow represents the in-plane component whereas the color lying between red and blue represents the angle made with the out-of-plane direction  $\hat{\mathbf{e}}_c$ , given by inverting  $\cos \theta_{\hat{\mathbf{e}}_c} = \mathbf{s} \cdot \hat{\mathbf{e}}_c = s^c$ . The phases in Figs. 2-5 feature either quadrupolar or octupolar moments but not both, whereas the phases in Figs. 6-13 each contain both quadrupolar and octupolar ordering which are stabilized due to the finite quadrupole-octupole interaction  $J_B$ .

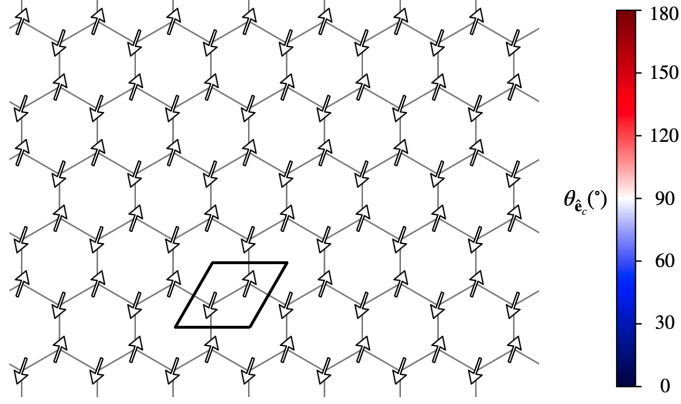


Figure 2. Pseudospin configuration at  $(\theta/\pi, \phi/\pi, J_B/\bar{J}) = (0.25, 0.25, 0.0)$  located within the AFQ phase. The colorbar, which indicates the size of the octupolar moment, applies to Figs. 2-13.

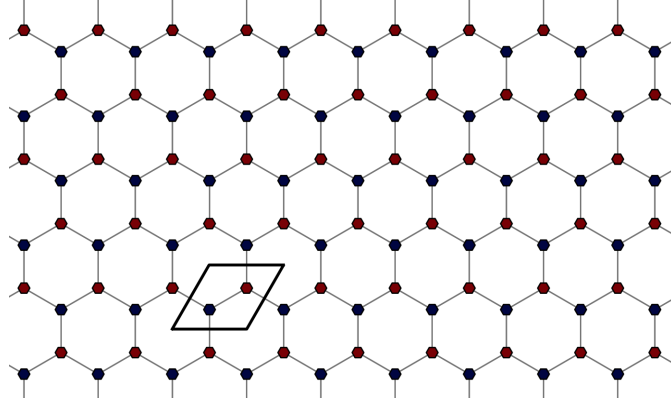


Figure 3. Pseudospin configuration at  $(\theta/\pi, \phi/\pi, J_B/\bar{J}) = (0.25, 0.5, 0.0)$  located within the AFO phase.

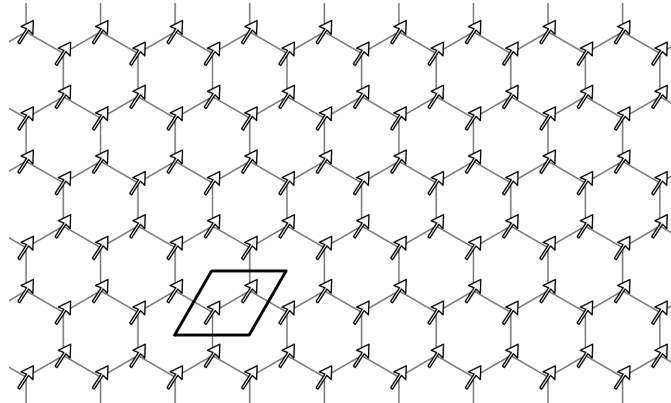


Figure 4. Pseudospin configuration at  $(\theta/\pi, \phi/\pi, J_B/\bar{J}) = (0.375, 1.0, 0.0)$  located within the FQ phase.

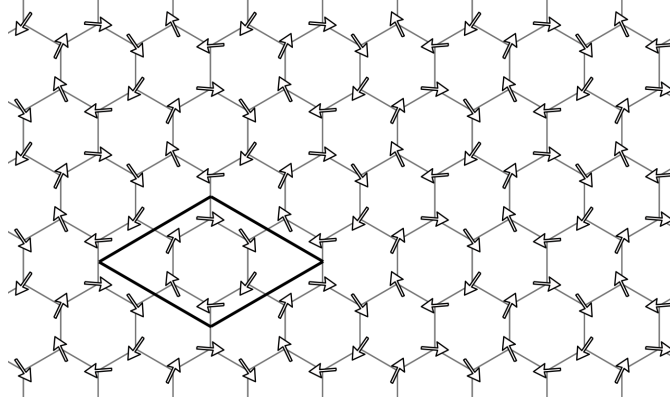


Figure 5. Pseudospin configuration at  $(\theta/\pi, \phi/\pi, J_B/\bar{J}) = (0.125, 1.0, 0.0)$  located within the VQ phase.

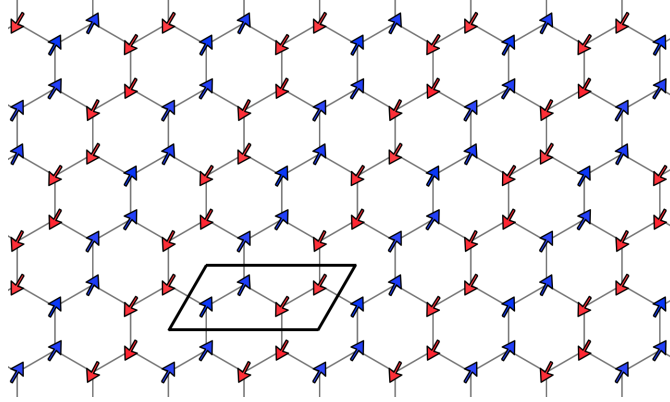


Figure 6. Pseudospin configuration at  $(\theta/\pi, \phi/\pi, J_B/\bar{J}) = (0.25, 1.0, 1/\sqrt{5})$  located within the ZZ phase.

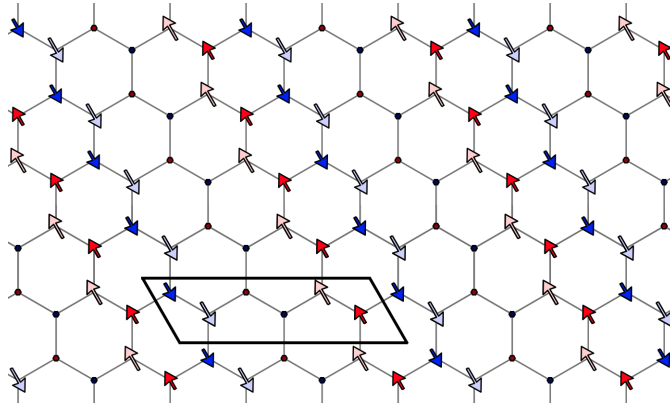


Figure 7. Pseudospin configuration at  $(\theta/\pi, \phi/\pi, J_B/\bar{J}) = (0.25, 0.8, 1/\sqrt{5})$  located within the 6-site phase.

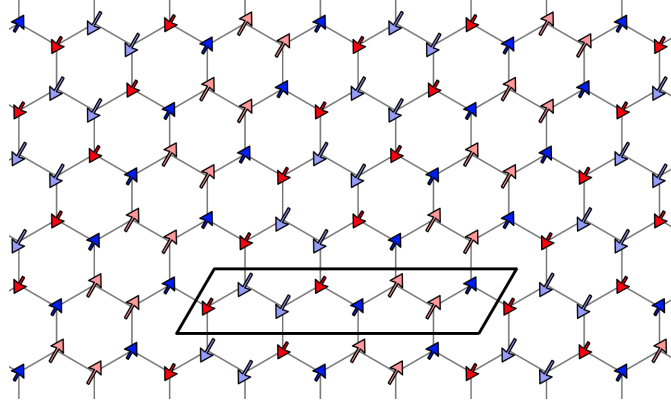


Figure 8. Pseudospin configuration at  $(\theta/\pi, \phi/\pi, J_B/\bar{J}) = (0.375, 0.175, 1/\sqrt{5})$  located within the  $8_I$  phase.

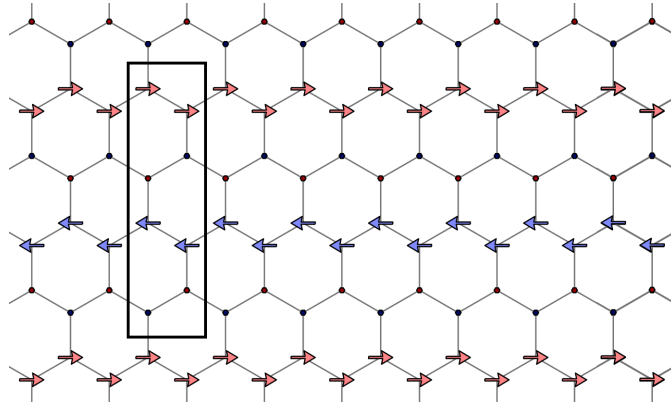


Figure 9. Pseudospin configuration at  $(\theta/\pi, \phi/\pi, J_B/\bar{J}) = (0.35, 0.765, 1/\sqrt{5})$  located within the  $8_{II}$  phase.

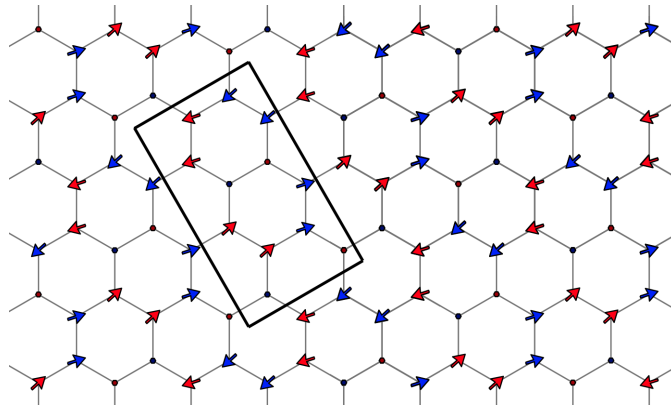


Figure 10. Pseudospin configuration at  $(\theta/\pi, \phi/\pi, J_B/\bar{J}) = (0.25, 0.72, 1/\sqrt{5})$  located within the  $12_I$  phase.



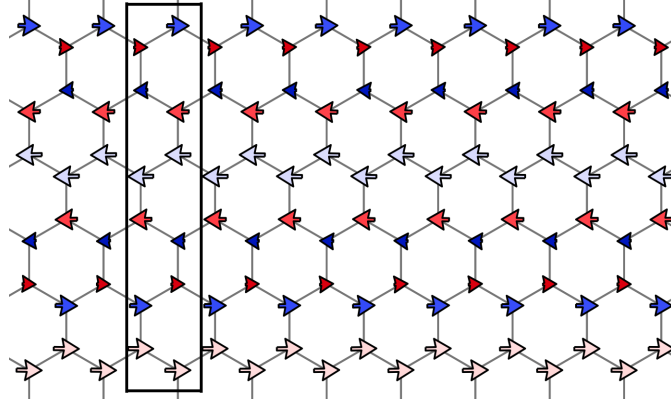


Figure 11. Pseudospin configuration at  $(\theta/\pi, \phi/\pi, J_B/\bar{J}) = (0.5, 0.81, 1/\sqrt{5})$  located within the  $12_{II}$  phase.

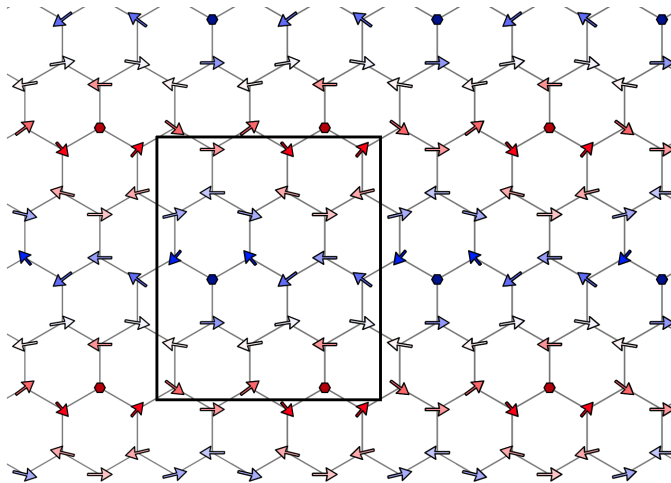


Figure 12. Pseudospin configuration at  $(\theta/\pi, \phi/\pi, J_B/\bar{J}) = (0.04, 0.5, 1/\sqrt{5})$  located within the 24-site phase.

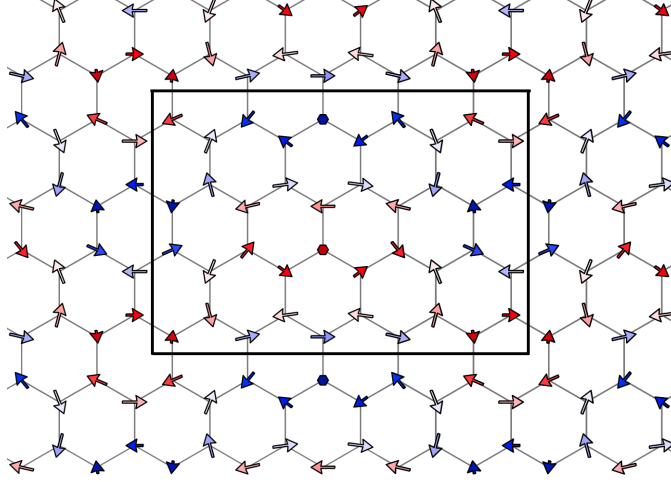


Figure 13. Pseudospin configuration at  $(\theta/\pi, \phi/\pi, J_B/\bar{J}) = (0.0, 0.0, 1/\sqrt{5})$  located within the 40-site phase.

## B. Phases in the quantum model

Let us recall that the quantum phase diagram in Fig. 4 of the main text is parameterized by  $(\xi, h_{\text{eff}})$  at fixed  $J_Q = 0$  and  $J_\tau = 1$ , where  $\xi = (J_B - J_O) / (J_B + J_O)$  and is restricted to  $-1 \leq \xi \leq 1$ ; in other words, tuning  $\xi$  is equivalent to tuning the ratio  $J_B/J_O = (1 + \xi) / (1 - \xi)$ . The  $\mathcal{H}\Phi$  package provides the real-space correlation functions  $\langle s_i^{\bar{\alpha}} s_j^{\bar{\beta}} \rangle = \langle \Psi | s_i^{\bar{\alpha}} s_j^{\bar{\beta}} | \Psi \rangle$  for  $\bar{\alpha}, \bar{\beta} \in \{a, b, c\}$ , where  $|\Psi\rangle$  is the ground state of the pseudospin model and  $i, j$  are sites on the 24-site cluster [10]. Let us define the quantity

$$T_{\mathbf{k}}^{\bar{\alpha}\bar{\beta}} = \frac{1}{N} \sum_{ij} \langle s_i^{\bar{\alpha}} s_j^{\bar{\beta}} \rangle e^{-i\mathbf{k}\cdot(\mathbf{r}_i - \mathbf{r}_j)} \quad (20)$$

in analogy with the spin structure factor. The octupolar and quadrupolar structure factors are then given by  $T_{\mathbf{k}}^O \equiv T_{\mathbf{k}}^{cc}$  and  $T_{\mathbf{k}}^Q \equiv T_{\mathbf{k}}^{aa} + T_{\mathbf{k}}^{bb}$ , and a signature of a long-range ordered phase are sharp peaks at some  $\mathbf{k} = \mathbf{k}^*$ , where  $\mathbf{k}^*$  are the corresponding ordering wavevectors. In the quantum phase diagram we find four phases: AFO, AFQ, ZZ, and KML. The first three are ordered with ordering wavevectors at  $\mathbf{k} = \Gamma'$  for both AFO and AFQ and  $\mathbf{k} = M$  for the ZZ phase, see Figs. 14-16. On the other hand, the KML is characterized by broad features in both  $T_{\mathbf{k}}^Q$  and  $T_{\mathbf{k}}^O$ , indicating a lack of long-ranged multipolar order. Moreover, both AFO and AFQ feature sharp peaks in only one of  $T_{\mathbf{k}}^Q$  and  $T_{\mathbf{k}}^O$  as shown in Figs. 14 and 15. On the other hand, both the KML and ZZ phases feature a combination of quadrupolar

and octupolar correlations.

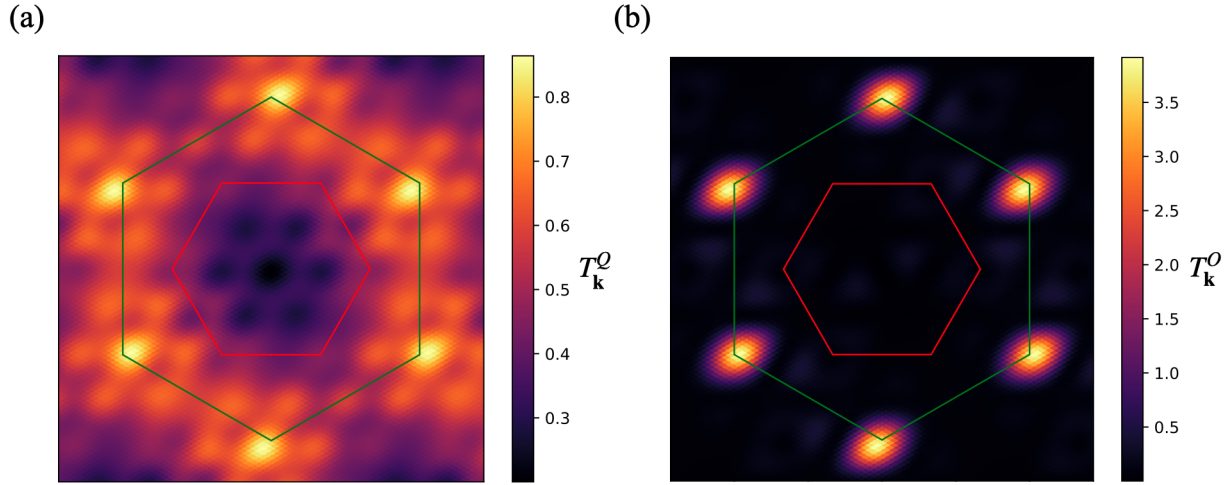


Figure 14. (a) Quadrupolar and (b) octupolar structure factors of ground state obtained at  $(\xi, h_{\text{eff}}) = (-1.0, 0.0)$  located within the AFO phase. For Figs. 14-16 the 1<sup>st</sup> and 2<sup>nd</sup> crystal Brillouin zones are shown in red and green respectively.

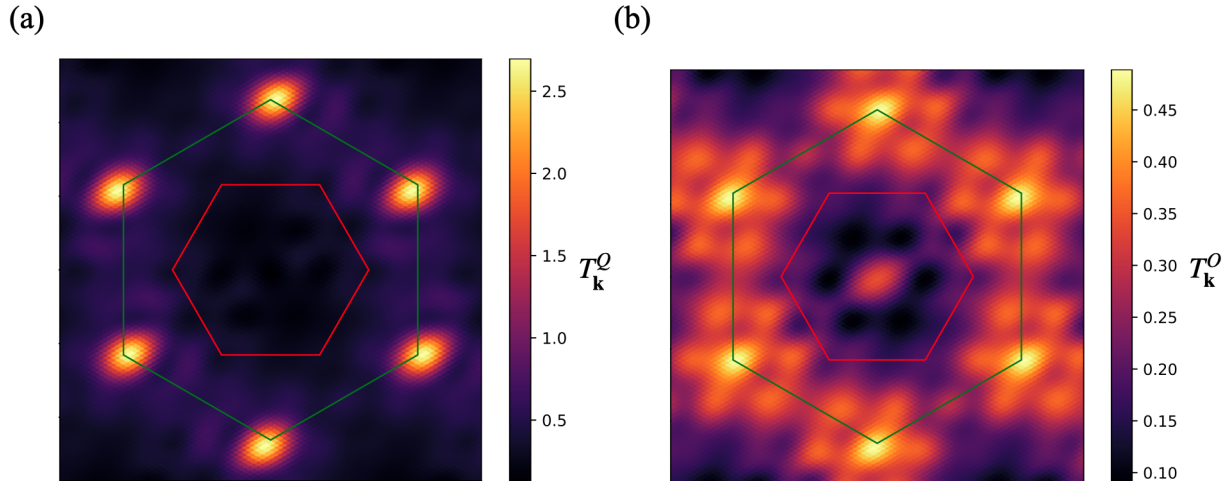


Figure 15. (a) Quadrupolar and (b) octupolar structure factors of ground state obtained at  $(\xi, h_{\text{eff}}) = (-0.15, 0.5)$  located within the AFQ phase. The presence of a small peak in  $T_{\mathbf{k}}^O$  at the  $\mathbf{k} = \Gamma$  point indicates the presence of ferro-octupolar correlations due to the finite  $h_{\text{eff}}$ .

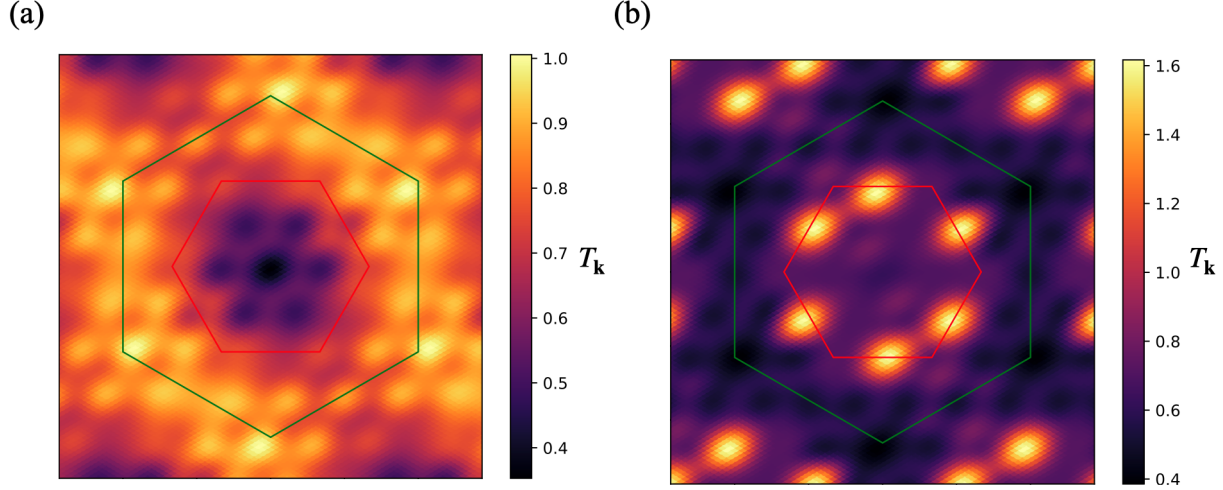


Figure 16. Combined quadrupolar and octupolar structure factor  $T_{\mathbf{k}} = T_{\mathbf{k}}^Q + T_{\mathbf{k}}^O$  at (a)  $(\xi, h_{\text{eff}}) = (0.0, 0.0)$  located within the KML phase, and (b)  $(\xi, h_{\text{eff}}) = (1.0, 0.0)$  located within the ZZ phase.

---

\* hykee@physics.utoronto.ca

- [1] A. Paramakanti, D. D. Maharaj, and B. D. Gaulin, Phys. Rev. B **101**, 054439 (2020).
- [2] S. Voleti, D. D. Maharaj, B. D. Gaulin, G. Luke, and A. Paramakanti, Phys. Rev. B **101**, 155118 (2020).
- [3] J. G. Rau, E. K.-H. Lee, and H.-Y. Kee, Phys. Rev. Lett. **112**, 077204 (2014).
- [4] D. Churchill and H.-Y. Kee, Phys. Rev. B **105**, 014438 (2022).
- [5] A. Messiah, *Quantum Mechanics, Volume II* (North-Holland, Amsterdam, 1965).
- [6] N. Metropolis, A. W. Rosenbluth, M. N. Rosenbluth, A. H. Teller, and E. Teller, The Journal of Chemical Physics **21**, 1087 (1953).
- [7] S. Kirkpatrick, C. D. Gelatt, and M. P. Vecchi, Science **220**, 671 (1983).
- [8] S. Kirkpatrick, Journal of Statistical Physics **34**, 975 (1984).
- [9] A. Rayyan, Q. Luo, and H.-Y. Kee, Phys. Rev. B **104**, 094431 (2021).
- [10] M. Kawamura, K. Yoshimi, T. Misawa, Y. Yamaji, S. Todo, and N. Kawashima, Computer Physics Communications **217**, 180 (2017).